2019 IEEE 30th Annual International Symposium on Personal, Indoor and Mobile Radio Communications (PIMRC): Track 3: Mobile and Wireless Networks

A Study of Sojourn Time for Indoor LiFi Cellular Networks

Mohammad Dehghani Soltani, Zhihong Zeng, Hossein Kazemi, Cheng Chen, Harald Haas and Majid Safari
LiFi Research and Development Centre, School of Engineering, University of Edinburgh, Edinburgh, UK
emails: {m.dehghani, zhihong.zeng, h.kazemi, cheng.chen, h.haas, majid.safari}@ed.ac.uk

***Abstract*—Sojourn time is an important parameter in the analysis and design of mobile cellular networks. It shows the expected time that a user equipment (UE) remains connected to the serving access point (AP) while moving in the network, i.e. stays within one cell. Therefore, an accurate estimation of the sojourn time is an essential element for mobility management. In this study, an analysis of the sojourn time for indoor light-fidelity (LiFi) cellular networks is presented based on the random waypoint (RWP) mobility model. It is initially assumed that the UE is oriented vertically upward and closed-form analytical expressions are derived. Monte-Carlo simulations are also provided to validate the analytical derivations and to gain more insight into the performance with different orientations. It is shown that the sojourn time mainly varies depending on the speed of the user. However, other factors such as the device orientation and the coverage area of cells also play a role in determining the sojourn time. The results offer several insights and design guidelines in consideration of this parameter for indoor LiFi networks.**

***Index Terms*—Sojourn time, light-fidelity (LiFi), handover, random waypoint (RWP).**

I. Introduction

Light-fidelity (LiFi) is an emerging wireless access technology that supports bidirectional communication and multiuser networking by means of light [1]. LiFi is seen as a green technology since it relies upon energy efficient light emitting diode (LED) luminaires in the existing lighting infrastructure. When multiple LED luminaires are put together, a LiFi cellular network is formed. Each LiFi access point (AP) provides broadband connectivity for multiple user equipment (UE) within its service area. On the one hand, the coverage area of a single LiFi cell is in the order of a few meters [2]. On the other hand, mobile users need seamless connectivity while moving between these small cells. This is especially crucial if the handover overhead is comparable to the amount of time that the user is expected to spend in a cell. Such a duration is referred to as sojourn time and it is an important factor in the characterization of user mobility in cellular networks [3].

The sojourn time has found diverse applications from mobility management to load balancing and user velocity estimation [4], [5]. Moreover, it is considered as a performance metric for resource allocation and quality-of-service (QoS) assessment [6]. Furthermore, the sojourn time is an indicator of the long term statistics of the user mobility, which can be used to reduce the signaling overhead in location-based services [7]. From a system-level standpoint, a short sojourn time leads to initiating two consecutive handovers for a UE when entering and leaving the cell. Fast algorithms are therefore required to support the UE QoS. These concepts are addressed in 4G long term evolution (LTE) standards using a threshold signal strength rule [8].

Sojourn time, also known as dwell time or residence time, has been widely studied in the context of radio frequency (RF) cellular networks [9]–[12]. The work in [9] provides an analysis of the sojourn time for circular microcells in a heterogeneous RF cellular network with the aim of devising a handover decision criterion based on the sojourn time. The authors of [10] have studied the sojourn time in order to address the relationship between three classes of mobility models including aimless, preferred direction and completely directed. They have identified two categories for the sojourn time: a new call sojourn time and handover sojourn time. The former describes the amount of time the UE spends in the call-initiated cell before it crosses the cell boundary. The latter specifies the time that it takes for the UE to stay in a cell to which an ongoing call of the UE is handed over. In [11], an analytical model of the sojourn time was presented for the overlapping area of two neighbouring cells. The model was developed under the assumption that the cell sojourn time follows an exponential distribution. Later in [12], the authors have shown that a hyper Erlang distribution better fits the sojourn time data for the overlapping area.

The above mentioned studies of the sojourn time are for RF cellular networks, mostly for outdoor scenarios. To the best of the authors' knowledge, there is no analytical study of the sojourn time for indoor LiFi networks. In this paper, we present an analytical study of the sojourn time for indoor LiFi cellular networks based on a random waypoint (RWP) mobility model. This is the first study concerning the sojourn time that considers unique characteristics of the LiFi channel model including the constraint of network boundaries (i.e., walls) on user mobility. Furthermore, the effect of the device orientation on the mean sojourn time is evaluated through Monte-Carlo simulations.

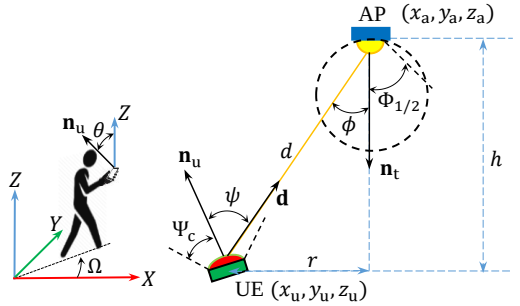

Fig. 1: The geometry of channel gain for a LiFi system.

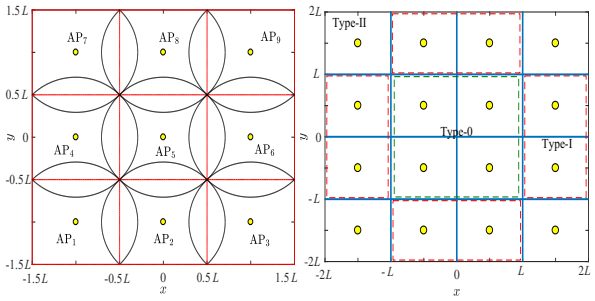

(a) 9 APs (b) 16 APs

Fig. 2: Square cell deployment

Notations: The symbols $\cdot$ and $\|\cdot\|$ denote the inner product and the Euclidean norm operators; $(\cdot)^{\mathrm{T}}$ denotes the transpose operator; $\mathbb{E}[\cdot]$ and $\tan^{-1}(y/x)$ represent the expectation and the four-quadrant inverse tangent.

II. System Description

An indoor LiFi network is considered in this study. In LiFi networks, the channel gain primarily depends upon the distance of the UE from the serving AP and its orientation [13], [14]. The geometry of the line-of-sight (LoS) downlink in a LiFi system is shown in Fig. 1. The DC gain of the LoS link is given by [13]:

$$H = \frac{(m+1)A}{2\pi d^2} \cos^m\phi \ \cos\psi \ \mathrm{rect}\left(\frac{\psi}{\Psi_c}\right), \quad (1)$$

where A, ϕ and ψ are the physical area of the detector; the angle of radiance with respect to the axis normal to the transmitter surface; and the angle of incidence with respect to the axis normal to the receiver surface, respectively. In addition, $m = -1/\log_2(\cos\Phi_{1/2})$ is the Lambertian order, with $\Phi_{1/2}$ denoting the half-intensity angle. The last factor in (1) accounts for an indicator function defined as $\mathrm{rect}(\frac{\psi}{\Psi_c}) = 1$ for $0 \le \psi \le \Psi_c$, and 0 otherwise, where Ψ_c represents the receiver field of view (FoV). The radiance angle ϕ at the transmitter and ψ the incidence angle at the receiver can be calculated by using the cosine rules from analytical geometry as $\cos\phi = -\mathbf{d}\cdot\mathbf{n}_t/\|\mathbf{d}\|$ and $\cos\psi = \mathbf{d}\cdot\mathbf{n}_u/\|\mathbf{d}\|$, where $\mathbf{n}_t = [0,0,-1]^{\mathrm{T}}$ and $\mathbf{n}_u$ are the normal vectors of the transmitter and the receiver planes, respectively, and $\mathbf{d}$ denotes the distance vector pointing from the receiver at the transmitter. Let the locations of the UE and the AP be denoted by (x_u, y_u, z_u) and (x_a, y_a, z_a), respectively. Then, $\mathbf{d} = [x_a - x_u, y_a - y_u, z_a - z_u]^{\mathrm{T}}$.

Consider a Cartesian coordinate system with X-Y axes on the horizontal plane as depicted in Fig. 1. The spatial directions of a user when moving on the X-Y plane can be characterized by two principal angles: the polar angle Ω which shows the direction of movement with respect to the X-axis and the tilt angle θ which signifies the orientation of the UE device with respect to the Z-axis, i.e. the angle between $\mathbf{n}_u$ and the Z-axis, see Fig. 1. To incorporate the link geometry into the RWP mobility model, it is convenient to express the normal vector $\mathbf{n}_u$ in terms of the angles θ and Ω. This is given by $\mathbf{n}_u = [-\sin\theta\cos\Omega, -\sin\theta\sin\Omega, \cos\theta]^{\mathrm{T}}$ [15]. Then, the LoS channel gain in (1) can be represented as [16]:

$$H = \frac{H_0}{d^{m+3}} \left(\lambda_1 \sin\theta + h\cos\theta \right) \mathrm{rect}\left(\frac{\psi}{\Psi_c}\right), \quad (2a)$$

$$\lambda_1 = r\cos\left(\Omega - \tan^{-1}\left(\frac{y_u - y_a}{x_u - x_a}\right)\right), \quad (2b)$$

where $H_0 = \frac{(m+1)Ah^m}{2\pi}$; r and h are the horizontal and vertical distances between the UE receiver and the AP, respectively. Note that for $\theta = 0$, i.e. a vertically upward orientation, the channel gain is just a function of d, while for $\theta \neq 0$, the channel gain depends on both d and Ω.

A. Cell Deployment

To form a LiFi cellular network, multiple optical APs are arranged with different deployments. A common deployment takes the regular form of a square lattice in which the APs are located on the vertices of a square grid. This is consistent with the square shape of indoor environments. For a downlink scenario, multiple LEDs are installed on the ceiling to transmit signals to UEs. Besides a square grid, other types of cell deployment include both hexagonal and Poisson point process (PPP) models. A study of downlink LiFi networks in [2] demonstrates that the use of hexagonal and PPP leads to the upper and lower bounds on the network performance concerning the received signal-to-interference-plus-noise ratio (SINR) and cell data rate.

The square lattice considered in this study is illustrated in Fig. 2a with 9 APs, and in Fig. 2b with 16 APs. According to Fig. 2b, cells are classified into three types based on their proximity to the network boundaries: Type-0 cells which are not bounded by any wall whatsoever; Type-I cells indicating those bounded by a wall from one side; and Type-II cells that are bounded with walls from two sides. With 9 APs as shown in Fig. 2a, there are four Type-I and Type-II cells in the network while there is only one Type-0 cell. When the network involves 16 APs as shown in Fig. 2b, there are equally four cells of Type-0 and those of Type-II, but there are eight cells of Type-I.

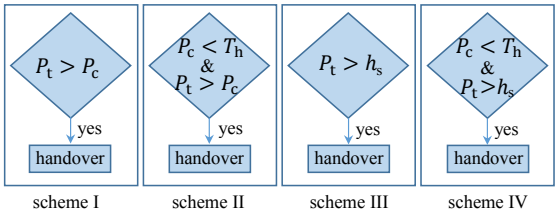

Fig. 3: Handover decision criteria.

B. Handover Decision Criteria

In principle, there are four criteria for a hard handover decision (HHD) based on the received signal strength (RSS) [17]: i) RSS alone; ii) RSS with a threshold; iii) RSS in conjunction with a hysteresis; and iv) RSS with both a threshold and a hysteresis. Let $P_{\rm c}$ and $P_{\rm t}$ denote the RSS values of the current and target APs, respectively. Note that $P_{\rm c}$ and $P_{\rm t}$ depend on the location and orientation of the UE. Furthermore, let T_0 be defined as the threshold RSS where the RSS values of the current and target APs coincide.

In the first HHD scheme, the UE is handed over from the current AP to the target AP if the signal strength of the target AP is greater than that of the current AP. In the second HHD scheme, a handover occurs if $P_{\rm c} < T_{\rm h}$ and $P_{\rm t} > P_{\rm c}$, where $T_{\rm h}$ is the handover threshold. Note the proper choice of $T_{\rm h}$ is quite critical and it can affect the system performance to a large extent. If $T_{\rm h} > T_0$, this scheme is the same as the first HHD one. Otherwise, the UE defers its handover until $P_{\rm c}$ falls below $T_{\rm h}$, i.e. $P_{\rm c} < T_{\rm h}$. In the third HHD scheme, the handover is performed if $P_{\rm t} > h_{\rm s}$, where $h_{\rm s}$ is the hysteresis value. The use of hysteresis assists in alleviating the ping-pong effect, due to repeated handovers between APs. The forth HHD scheme is a combination of the second and third ones, whereby a handover takes place when the conditions $P_{\rm c} < T_{\rm h}$ and $P_{\rm t} > h_{\rm s}$ are simultaneously satisfied. For convenience, the operation principles of all four schemes are summarized in Fig. 3.

In this study, the focus is put on the first and second HHD schemes due to the space limitation. The analysis of the third and forth HHD schemes will be carried out in our future research. A geometric interpretation of the first two schemes is provided with the aid of Fig. 2b. Note that the handover boundaries of the first HHD scheme are indicated by red lines, while black arcs show the boundaries of the threshold-based HHD according to the second scheme.

C. Receiver Mobility Model

This section describes the underlying RWP mobility model which is adopted from [18]. According to the RWP model, intermediate points on the way are referred to as waypoints. At each waypoint, the step that a mobile user intends to take needs to fulfill certain properties before moving to the next waypoint, including i) the destinations or waypoints are chosen uniformly at random with a probability of $1/a^2$, where a is the side length of room; ii) the movement path is a straight line; and iii) the speed is constant during the movement.

Such a movement process is mathematically expressed by an infinite sequence of triples: $\{(\mathbf{P}_{n-1}, \mathbf{P}_n, v_n)\}_{n\in\mathbb{N}}$, where n denotes the nth movement period during which the UE proceeds between the current waypoint $\mathbf{P}_{n-1} = (x_{n-1}, y_{n-1}, 0)$ and the upcoming waypoint $\mathbf{P}_n = (x_n, y_n, 0)$ with a constant velocity $V_n = v$. This model has been used in LiFi networks to analyse the performance of mobile users, e.g. [19]–[21].

In the next section, we derive analytical expressions of the sojourn time for a vertically upward oriented UE.

III. Sojourn Time Analysis

The mean cell sojourn time for a mobile node is defined as the amount of time that the mobile node is expected to spend in a particular cell before leaving that cell. This depends on factors such as the velocity of users and their traversed path, and the shape and size of cells. Let $\{X(t,\xi), t \geq 0\}$ denote a stochastic process, with the time variable t; and the domain ξ showing the set of all outcomes, i.e. $\xi \in \{\xi_1, \xi_2, \cdots, \xi_K\}$, where K is the total number of possible outcomes. Also, let $\tau(\xi_i)$ show the total time that the user expends with a given outcome ξ_i. The aim is to acquire the expected value of $\tau(\xi_i)$, which can be obtained as follows [22]:

$$\mathbb{E}[\tau(\xi_i)] = \lim_{M\to\infty} \frac{\tau(\xi_i)}{M}, \tag{3}$$

where M is the total number of events. Note that (3) is a general definition which is independent of the user mobility model, device orientation and cell deployment. Based on (3), the authors in [3] have proposed a tractable method to compute the sojourn time of RWP analytically, regardless of the cell shape. It follows that:

$$S_{\rm T} = \mathbb{E}[T] \int_{\mathcal{C}} \Pr(\mathrm{d}A(x,y)), \tag{4}$$

where $\mathbb{E}[T]$ is the expected transition time which is defined as the average duration of moving between two successive waypoints; $\mathcal{C}$ denotes the set of points corresponding to the cell coverage area; and $\mathrm{d}A(x,y)$ is a differential element of the room area evaluated at the point (x,y). The expected transition time can be calculated as $\mathbb{E}[T] = \mathbb{E}[\mathcal{L}]/v$, where $\mathbb{E}[\mathcal{L}]$ is the expected transition length. According to [23], for a square room of length a, $\mathbb{E}[\mathcal{L}] = 0.5214a$. Therefore, the expected transition time can be expressed in the following form:

$$\mathbb{E}[T] = \frac{0.5214a}{v}. \tag{5}$$

In (4), $\Pr(\mathrm{d}A(x,y))$ is the probability that the UE resides within the set $\mathrm{d}A(x,y)$ during the course of movement from $\mathbf{P}_{n-1}$ to $\mathbf{P}_n$. This probability can be approximated as [23]:

$$\Pr(\mathrm{d}A(x,y)) \approx f_{XY}(x,y)|\mathrm{d}A(x,y)|, \tag{6}$$

where $f_{XY}(x,y)$ is the probability density function of the spatial node distribution; and $|\mathrm{d}A(x,y)|$ is the area of $\mathrm{d}A(x,y)$. The function $f_{XY}(x,y)$ is given by [18]:

$$f_{XY}(x,y) \approx \frac{36}{a^6}(x^2-\frac{a^2}{4})(y^2-\frac{a^2}{4}). \tag{7}$$

Finally, substituting (5), (6) and (7) into (4), the expected sojourn time of the RWP mobility model for a cell with coverage area $\mathcal{C}$ can be approximated as:

$$S_{\mathrm{T}} \approx \frac{0.5214a}{v}\mathcal{A}_{\mathrm{c}}, \tag{8}$$

where $\mathcal{A}_{\mathrm{c}}$ is given by:

$$\mathcal{A}_{\mathrm{c}} = \frac{36}{a^6}\iint_{\mathcal{C}}(x^2-\frac{a^2}{4})(y^2-\frac{a^2}{4})\mathrm{d}x\mathrm{d}y. \tag{9}$$

Note that the notion of the remaining sojourn time has also been described and analyzed in [9]. It is defined as the expected time from the moment that the call is initiated until the moment that the user exits the call-initiated cell. In this study, however, we focus only on the cell sojourn time. Based on (8), the AP can have an acceptable estimation of the sojourn time by knowing the average UE's speed, which can be fed back to the AP by means of a limited-feedback mechanism [24], [25].

Case Study: Vertically Upward UE

This section evaluates the expected sojourn time for a vertically upward oriented UE in a square network shown in Fig. 2a. First, scheme I is considered for handover execution. Let N denote the total number of cells. The room of size $a \times a$ is divided into N equal squares with a length of L. Without loss of generality, it is assumed that the origin of the coordinate system is at the center of room. In this case, if N is odd, the coordinates of cells span from $(2i-1)L/2$ to $(2i+1)L/2$ in the x-direction and from $(2j-1)L/2$ to $(2j+1)L/2$ in the y-direction, where $i,j \in \{0,\pm1,\cdots,\pm\frac{\sqrt{N}-1}{2}\}$. Thus, the integral in (9) is derived in closed form as:

$$\begin{aligned}\mathcal{A}_{\mathrm{c}} &= \frac{36}{a^6}\int_{(2i-1)\frac{L}{2}}^{(2i+1)\frac{L}{2}}\int_{(2j-1)\frac{L}{2}}^{(2j+1)\frac{L}{2}}(x^2-\frac{a^2}{4})(y^2-\frac{a^2}{4})\mathrm{d}x\mathrm{d}y \\ &= \frac{(3a^2L-(12i^2+1))L^3))(3a^2L-((12j^2+1))L^3))}{4a^6} \\ &= \frac{(3N^2-(12i^2+1))(3N^2-(12j^2+1))}{4N^3}.\end{aligned} \tag{10}$$

The last equality is due to the fact that $a = \sqrt{N}L$. In the case where N is even, the coordinates of cells are extended across iL to $(i+1)L$ in the x-direction and between jL and $(j+1)L$ in the y-direction, where $i,j \in \{\frac{-\sqrt{N}}{2},\cdots,\frac{\sqrt{N}}{2}-1\}$. Hence, the integral in (9) is derived in closed form as:

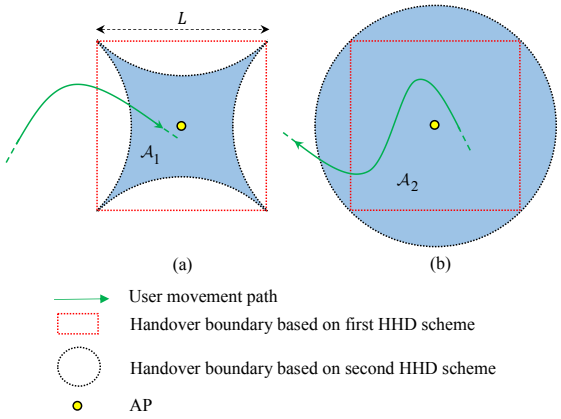

Fig. 4: Handover boundary of type 0 cell based on first and second HHD schemes.

$$\begin{aligned}\mathcal{A}_{\mathrm{c}} &= \frac{36}{a^6}\int_{iL}^{(i+1)L}\int_{jL}^{(j+1)L}(x^2-\frac{a^2}{4})(y^2-\frac{a^2}{4})\mathrm{d}x\mathrm{d}y \\ &= \frac{(3a^2L-4(3i(i+1)+1)L^3))(3a^2L-4(3j(j+1)+1)L^3))}{4a^6} \\ &= \frac{(3N-4(3i(i+1)+1))(3N-4(3j(j+1)+1))}{4N^3}.\end{aligned} \tag{11}$$

For the special case of $N = 9$ as shown in Fig. 2a, by using (8) and (10), the sojourn time expressions for Type-0, Type-I and Type-II cells, respectively, reduce to:

$$S_0 \approx 0.3626\frac{L}{v}, \tag{12a}$$

$$S_{\mathrm{I}} \approx 0.1953\frac{L}{v}, \tag{12b}$$

$$S_{\mathrm{II}} \approx 0.1051\frac{L}{v}. \tag{12c}$$

For the special case of $N = 16$ as shown in Fig. 2b, by using (8) and (11), the sojourn time expressions for the three cell types are simplified to:

$$S_{\mathrm{T}_0} \approx 0.2463\frac{L}{v}, \tag{13a}$$

$$S_{\mathrm{I}} \approx 0.112\frac{L}{v}, \tag{13b}$$

$$S_{\mathrm{II}} \approx 0.051\frac{L}{v}. \tag{13c}$$

Next, the sojourn time is evaluated under the second HHD scheme. There are two possible cases: i) when the user goes toward the cell, see Fig. 4a; and ii) when the user departs from the cell, see Fig. 4b. It can be seen in Fig. 4 that the coverage area of the cell *before* being handed over to the AP is less than L^2, and it is denoted by $\mathcal{A}_1$. By contrast, the coverage area of the cell *after* being handed over to the AP is larger than L^2, and it is denoted by $\mathcal{A}_2$. Both areas $\mathcal{A}_1$ and $\mathcal{A}_2$ need to be taken into account when calculating the mean sojourn time for the cell. This gives rise to:

$$S_{\mathrm{T}} \approx \frac{1}{2}\left(\frac{0.5214a}{v}\mathcal{A}_{\mathrm{c}_1} + \frac{0.5214a}{v}\mathcal{A}_{\mathrm{c}_2}\right), \qquad (14)$$

which, in fact, is the average sojourn time over the areas $\mathcal{A}_1$ and $\mathcal{A}_2$. In (14), $\mathcal{A}_{\mathrm{c}_1}$ and $\mathcal{A}_{\mathrm{c}_2}$ are given by:

$$\mathcal{A}_{\mathrm{c}_1} = \frac{36}{a^6}\iint_{\mathcal{A}_1}(x^2 - \frac{a^2}{4})(y^2 - \frac{a^2}{4})\mathrm{d}x\mathrm{d}y, \qquad (15a)$$

$$\mathcal{A}_{\mathrm{c}_2} = \frac{36}{a^6}\iint_{\mathcal{A}_2}(x^2 - \frac{a^2}{4})(y^2 - \frac{a^2}{4})\mathrm{d}x\mathrm{d}y. \qquad (15b)$$

The same approach can be utilized to compute the mean sojourn time for Type-I and Type-II cells.

IV. Simulation Results and Discussions

Numerical results are presented and compared them with the analytical results from Section III. Monte-Carlo simulations are conducted based on (4) with about 8000 iterations carried out for each result. A room of size 16×16 m^2 with 16 APs is considered. All APs have the same half-intensity angle of $\Phi_{1/2} = 60$. The vertical distance between the UE and the AP remains the same at $h = 2$ m during the movement. The receiver FOV is assumed to be $\Psi_{\mathrm{c}} = 90$. The PD area is $A = 10^{-4}$ m^2. The optical power of LEDs is always fixed at 1 W.

By assuming $v = 1$ m/s and $\theta = 0$, the mean sojourn time is computed based on the analytical expression in (13) and the resulting values are listed in Table I. The simulation results are also shown in Fig. 5. From the figure, the mean sojourn time for cells of Type-0, Type-I and Type-II are 0.96 s, 0.44 s and 0.25 s, respectively. Thus, the analytical results, given in Table I, are in good agreement with those obtained by the simulations. It can be inferred from these results that the user tends to stay more in Type-0 cells, whose sojourn time is almost four times that of Type-II cells. This suggests that the knowledge of the mean sojourn time at APs is beneficial for handover management and resource allocation.

Next, the sojourn time is assessed based on HHD with scheme II for different values of the threshold RSS, T_{h}. The results are presented in Fig. 6 for $\theta = 0$ and $\theta = 41°$. The value of θ is chosen based on experimental measurements of the device orientation for mobile users, see [14]). The value of T_{h} varies from 8.9×10^{-7} W to 1×10^{-7} W, which corresponds to cell radii of $2\sqrt{2}$ m and $4\sqrt{2}$ m, respectively. It can be observed that for $T_{\mathrm{h}} \leq 1.8 \times 10^{-7}$ W, increasing the threshold does not affect the sojourn time especially for type-II cells. Besides, the rate of increase in the sojourn time suddenly rises for $T_{\mathrm{h}} = 1 \times 10^{-7}$ W. An explanation for such a sharp increase can be given with the aid of Fig. 4a, as the blue area labeled by $\mathcal{A}_1$ becomes zero by choosing $T_{\mathrm{h}} = 1 \times 10^{-7}$ W.

Fig. 7 presents the effect of the tilt angle, θ, on the sojourn time for HHD schemes I and II. For scheme II, we set $T_{\mathrm{h}} = 8.9 \times 10^{-7}$ W. It is observed that the tilt angle does not notably influence the mean sojourn time for different cell types. Finally, the effect of the user velocity on the sojourn time is studied. According to (8), the mean sojourn time is inversely proportional to the user velocity, i.e. $S_{\mathrm{T}} \propto \frac{1}{v}$. Monte-Carlo simulations are presented in Fig. 8 for HHD with scheme I and II and $\theta = 0$. The results confirm the inverse relation between the user velocity and the sojourn time. It is noted that in these simulations for HHD with scheme II, we set $T_{\mathrm{h}} = 8.9 \times 10^{-7}$ W.

TABLE I: Analytical results of sojourn time in a room of size 16×16 m^2 with 16 APs with $v = 1$ m/s and $\theta = 0$.

Cell type	Type-0	Type-I	Type-II
Sojourn time	0.98 s	0.45 s	0.2 s

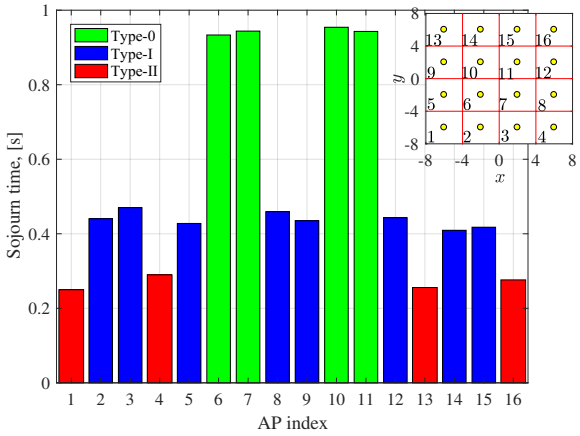

Fig. 5: Simulations of sojourn time for RWP mobility model in a room of size 16×16 m^2 with 16 APs.

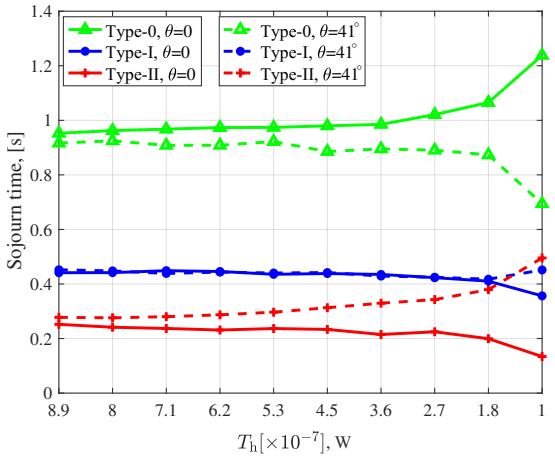

Fig. 6: Simulations of sojourn time based on HHD with scheme II versus different handover thresholds, T_{h}.

V. Conclusions

The sojourn time is a determining parameter in the design of mobile cellular networks. In this study, we considered analyzing and investigating the sojourn time for indoor LiFi cellular networks. More specifically, we derived the sojourn time analytically for the case where the UEs are oriented vertically upward. In addition,

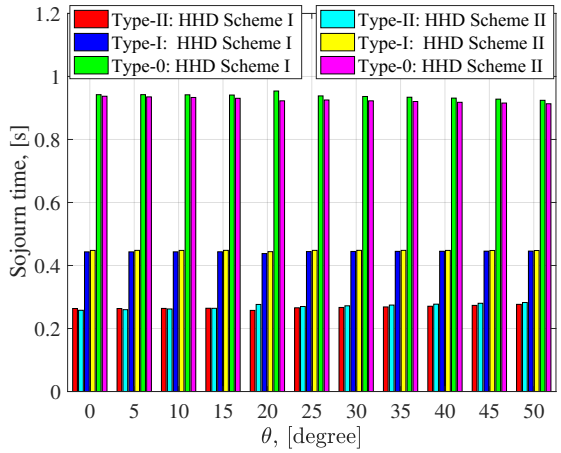

Fig. 7: Comparison of sojourn time obtained based on HHD with scheme I and scheme II for $v = 1$ m/s and different θ.

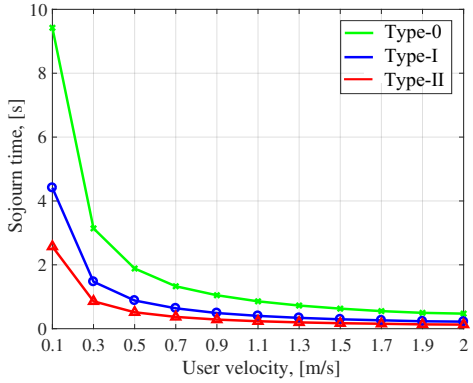

Fig. 8: Simulations of sojourn time for various velocity of UE and with $\theta = 0$. Markers and solid lines represent HHD with scheme I and HHD with scheme II, respectively.

Monte-Carlo simulations confirmed that the effect of the tilt angle on the sojourn time is insignificant. Moreover, the sojourn time was examined through the use of two RSS-based handover criteria in conjunction with the RWP mobility model. The results show that the user velocity is the main factor affecting the sojourn time. For future studies, we will apply the presented methodology to assess the sojourn time for hexagonal and PPP cell deployment models.

ACKNOWLEDGMENT

H. Haas gratefully acknowledges financial support by the Engineering and Physical Sciences Research Council (EPSRC) under an Established Career Fellowship grant EP/R007101/1 and grant EP/L020009/1 (TOUCAN).

REFERENCES

[1] H. Haas, L. Yin, Y. Wang, and C. Chen, "What is LiFi?" *J. Lightw. Technol.*, vol. 34, no. 6, pp. 1533–1544, Mar. 2016.

[2] C. Chen, D. A. Basnayaka, and H. Haas, "Downlink Performance of Optical Attocell Networks," *J. Lightw. Technol.*, vol. 34, no. 1, pp. 137–156, Jan. 2016.

[3] X. Lin *et al.*, "Towards Understanding the Fundamentals of Mobility in Cellular Networks," *IEEE Trans. Wireless Commun.*, vol. 12, no. 4, pp. 1686–1698, April 2013.

[4] G. Ning, G. Zhu, Q. Li, and R. Wu, "Dynamic Load Balancing Based on Sojourn Time in Multitier Cellular Systems," in *IEEE 63rd Veh. Technol. Conf. (VTC Spring)*, vol. 1, Melbourne, Australia, May 2006, pp. 111–116.

[5] A. Merwaday *et al.*, "Sojourn Time-Based Velocity Estimation in Small Cell Poisson Networks," *IEEE Commun. Lett.*, vol. 20, no. 2, pp. 340–343, Feb 2016.

[6] S. Shin, U. Lee, F. Dressler, and H. Yoon, "Analysis of Cell Sojourn Time in Heterogeneous Networks With Small Cells," *IEEE Commun. Lett.*, vol. 20, no. 4, pp. 788–791, April 2016.

[7] P. Baumann, W. Kleiminger, and S. Santini, "How Long Are You Staying? Predicting Residence Time from Human Mobility Traces," in *Proc. of the 19th Annu. Int. Conf. on Mobile Computing & Networking*, Miami, USA, 2013, pp. 231–234.

[8] "Evolved universal terrestrial radio access (e-utra): mobility enhancements in heterogeneous networks," 3GPP TR 36.8de V0.0.1, Tech. Rep., May 2011.

[9] K. L. Yeung and S. Nanda, "Channel Management in Microcell/Macrocell Cellular Radio Systems," *IEEE Trans. Veh. Technol.*, vol. 45, no. 4, pp. 601–612, Nov 1996.

[10] E. Jugl and H. Boche, "Dwell Time Models for Wireless Communication Systems," in *IEEE 50th Veh. Technol. Conf. (VTC Fall)*, vol. 5, 1999, pp. 2984–2988.

[11] V. Pla and V. Casares-Giner, "Effect of the Handoff Area Sojourn Time Distribution on the Performance of Cellular Networks," in *4th Int. Workshop on Mobile and Wireless Commun. Netw.*, Stockholm, Sweden,, Sep. 2002, pp. 401–405.

[12] ——, "Analytical-Numerical Study of the Handoff Area Sojourn Time," in *Proc. IEEE Globecom*, vol. 1, Taipei, Taiwan, Nov 2002, pp. 886–890.

[13] J. M. Kahn and J. R. Barry, "Wireless Infrared Communications," *Proc. IEEE*, vol. 85, no. 2, pp. 265–298, Feb. 1997.

[14] M. D. Soltani, A. A. Purwita, Z. Zeng, H. Haas, and M. Safari, "Modeling the Random Orientation of Mobile Devices: Measurement, Analysis and LiFi Use Case," *IEEE Trans. Commun.*, vol. 67, no. 3, pp. 2157–2172, Mar. 2019.

[15] M. D. Soltani, A. A. Purwita, I. Tavakkolnia, H. Haas, and M. Safari, "Impact of Device Orientation on Error Performance of LiFi Systems," *IEEE Access*, vol. 7, pp. 41 690–41 701, 2019.

[16] M. D. Soltani, "Analysis of Random Orientation and User Mobility in LiFi Networks," *The University of Edinburgh*, 2019.

[17] G. P. Pollini, "Handover rates in cellular systems: towards a closed form approximation," in *Proc. IEEE Globecom*, vol. 2, Phoenix, USA, Nov 1997, pp. 711–715.

[18] C. Bettstetter, H. Hartenstein, and X. Perez-Costa, "Stochastic Properties of the Random Waypoint Mobility Model," *ACM Wireless Netw.*, vol. 10, no. 5, pp. 555–567, Sep. 2004.

[19] M. D. Soltani, H. Kazemi, M. Safari, and H. Haas, "Handover Modeling for Indoor Li-Fi Cellular Networks: The Effects of Receiver Mobility and Rotation," in *IEEE Wireless Communications and Networking Conference (WCNC)*, San Fransisco, USA, March 2017, pp. 1–6.

[20] A. Gupta and P. Garg, "Statistics of SNR for an Indoor VLC System and its Applications in System Performance," *IEEE Commun. Lett.*, vol. 22, no. 9, pp. 1898 – 1901, Jul. 2018.

[21] M. A. Arfaoui, M. D. Soltani, I. Tavakkolnia, A. Ghrayeb, C. Assi, H. Haas, M. Hasna, and M. Safari, "SNR Statistics for Indoor VLC Mobile Users with Random Orientation," in *IEEE Int. Conf. Commun. Workshops (ICC Workshops)*, Shanghai, China, May 2019, pp. 1–6.

[22] L. Takics, "Sojourn Times," *Journal of Applied Mathematics and Stochastic Analysis*, vol. 9, no. 4, pp. 415–426, 1996.

[23] E. Hyytiä and J. Virtamo, "Random Waypoint Mobility Model in Cellular Networks," *Wireless Networks*, vol. 13, no. 2, pp. 177–188, 2007.

[24] M. D. Soltani, X. Wu, M. Safari, and H. Haas, "Bidirectional User Throughput Maximization Based on Feedback Reduction in LiFi Networks," *IEEE Trans. Commun*, vol. 66, no. 7, pp. 3172–3186, July 2018.

[25] M. D. Soltani, M. Safari, and H. Haas, "On throughput maximization based on optimal update interval in Li-Fi networks," in *IEEE Int. Symp. Pers., Indoor Mobile Radio Commun. (PIMRC)*, Oct 2017, pp. 1–6.